Preface

This book discusses how, in random media, light dramatically changes electron–electron interaction. Despite Coulomb repulsion, the effective interaction demonstrates attraction, even under strong pumping. Light (both coherent and natural) acts like an optical motor, transporting electrons in a direction opposite to that of the electric force direction: electric current flows against bias and static polarization is aligned in opposition to the applied electric field. The uncommon electron transport increases the initial perturbations and is the foundation of the light-driven structuring of a matter. This structuring belongs to the class of self-organization phenomena of open dissipative systems and exhibits a number of fascinating properties.

Light pushes electrons into spatially ordered macroscopic bunches observed in fused silica under ArF-laser irradiation. It carves material balls with fixed diameters equal to 2 microns and throws them out of the ablation crater. Moderate light intensity drills material, forming long channels that align with the wave vector and drill diameters can be as small as 2 microns, while the beam spot is a few millimeters.

Bicolor excitation causes orientational ordering in random media. We monitored the induced transformation by measuring the emerged second harmonic signal. The orientational ordering has been used for all optical poling of glasses. Light treatment prepares phase-matched grating of second-order nonlinear susceptibility and provides effective second harmonic generation. All optical poling was performed in bulk materials and fibers.

We give numerous examples of spatial, orientational and temporal ordering, and we present theoretical and experimental evidence of several kinds of light-driven self-organization. Ordering induced by natural light gives us an idea of how the life on Earth may have come about. The light-driven self-organization might have been the first, prebiotic stage in the chain events that gave rise to life.

We discuss electron acceleration driven by petawatt laser pulses. Particles are accelerated by an electric field of plasmon, generated by the laser. The laser wakefield electron accelerator opens new horizons in light-mediated manipulation by matter.

Troitsk, Moscow Region,
June 2008

Boris P. Antonyuk

2 Light-Driven Ordering: Theory

Light-driven *self-organization* belongs to a class of nice phenomena when order rises from chaos. It is a wonder, because we more often observe how order descends into chaos according to the law of entropy increase in closed thermodynamic systems. In the case of Zhabotinskii reactions, the chemical system can exhibit waves of concentration under constant flow of substances [2], while in the thermodynamic case only melancholy dissipation to a constant level is possible. Rayleigh–Benard convection provides an example of self-organization in a hydrodynamic system [1]. It rises when upper and lower surfaces of a layered oil are kept at different temperatures and the difference exceeds some threshold (heating is from the bottom). At small temperature difference, thermal energy is transferred through the oil by ordinary heat transport. When the difference reaches the threshold, phonons cannot carry large heat flow and nontrivial convection is triggered: ordered in space, convective cells are formed. The well-known Turing instability belongs to this family [3]. Two diffusion equations with nonlinear coupling exhibit transition to an inhomogeneous state, where concentrations form static waves. Similar phenomena are found in optics [4]. Zhabotinskii reactions and Rayleigh–Benard convection are examples of self-organization driven by flows of chemical substances or heat through a system, respectively. Here, we pay attention to phenomena of the same family driven by light transmitted through a system. Photon flux will be considered constant in space and time and plays a role similar to that of a violin bow, triggering self-organization in a system. Spatial and temporal scales of internal motion and ordering phenomena in a system are its intrinsic characteristics not connected with space and time scales of light field.

In contrast to our earlier discussion, thermodynamic diffusion light allows different molecules of a gas to shift in opposite directions and therefore allows a decrease in entropy. Kel'mukhanov and Shalagin [9, 10] proposed realization of Maxwell's demon separating molecules. If light frequency ω is shifted from the energy of an electron transition $\varepsilon/\hbar$, then only moving with some velocity $\mathbf{v}$ molecules interact with light (Doppler effect). These particles see the light wave

$$\begin{aligned}\mathbf{E}_0 \exp\bigl(\mathrm{i}\mathbf{k}\mathbf{R}(t) - \mathrm{i}\omega t\bigr) &= \mathbf{E}_0\bigl(\exp \mathrm{i}\mathbf{k}(\mathbf{R}_0 + \mathbf{v}t) - \mathrm{i}\omega t\bigr)\\ &= \mathbf{E}_0 \exp\bigl(\mathrm{i}\mathbf{k}\mathbf{R}_0 - \mathrm{i}(\omega - \mathbf{k}\mathbf{v})t\bigr)\end{aligned}$$

with the frequency $\omega - \mathbf{k}\mathbf{v}$. Radius vector $\mathbf{R}(t)$ points the molecule position. The velocity of the resonance (and therefore excited) particles is determined from the

equation

$$\hbar(\omega - \mathbf{kv}) = \varepsilon.$$

The symmetric portion of the molecules with the velocity $-\mathbf{v}$ is out of resonance and therefore not excited. Cross-sections of the impact interaction of excited and unexcited particles with buffer gas are different, therefore the active molecules push buffer gas along the line of the wave propagation in the direction depending on the energy mismatch $\hbar\omega - \varepsilon$. Buffer gas, in its turn and according to Newton's third law, pushes the active molecules in the reverse direction. So light separates active and buffer gas molecules in space, producing a low entropy state.

The discussed phenomenon takes place even for a single active atom in a buffer gas. Due to collision, it changes velocity and moves within Doppler's distribution. The atom interacts with light when resonance conditions are fulfilled. It pushes buffer gas differently at the resonance velocity $\mathbf{v}$ and in symmetric state $-\mathbf{v}$ and therefore suffers reaction shifting, the atom in opposite direction to the buffer gas shift. So, this is a single-particle effect and may be called light-driven *organization* of a matter. Here I deal with the collective effects similar to phase transitions belonging to the class of light-driven *self-organization*.

Our interest here is in light-induced transitions between local electron states. Normally frequency dependence of the corresponding absorption line is given by the Lorenz curve. This is true for the cases when other degrees of freedoms are not involved in process. Electron transitions between different potential wells are of a special interest. Electrons gain energy in this case and shift in space. The excited state may be treated as an electron–hole pair in the final and initial potential wells, respectively. Coulomb interaction contributes to the energy of the separated charges and it depends considerably on the distance between particles, i.e. on the vibration modes. Electron transitions in this case are accompanied by phonon emission: the main part of the absorbed photon energy (≈ 1 eV) gains electrons and the minor part (≈ 0.01 eV) gains phonons. The absorption band in this case consists of a sharp Lorenz electron part and broad phonon wings [11]. An increase in the electron–phonon coupling results in a decrease of the electron line and an increase of the phonon band. In the case of strong electron–phonon coupling (namely this is realized in the systems discussed here) the absorption band has Gauss form. The maximum of this band exceeds the electron energy ε to the value of so-called Stokes shift $A \approx 0.01$ eV and corresponds to the emitted phonon energy. Line width $\Delta \approx 0.01$ eV is determined by the same factor and means that any of the phonons with the energy $0 \div \Delta$ may be emitted.

2.1 Ordering in Molecular Crystals

2.1.1 Spatial Ordering

In order to explain the main idea of my model of light-driven self-organization, let us consider a molecular crystal containing a donor–acceptor pair in each unit cell

under the action of a laser wave that is homogeneous in space and time. Electrons transit from donor to acceptor, absorbing one laser photon and in return emitting a photon or phonon. Due to electron–hole separation, this charge transfer exciton (CTE) acts like a spring, deforming the lattice (strong exciton–phonon coupling). This distortion results in large effective mass. This in turn prevents the CTE motion and the exciton decays at the same point where it was created. Nevertheless ordering is possible, as we shall see in the following (the idea was published in [12]).

The generation rate of the first exciton is the same for each unit cell and, according to [11], is

$$W = I\sigma_0 \exp\left[-(\hbar\omega - \varepsilon_0 - A)^2/\Delta^2\right],$$

where I stands for photon flux, $\sigma_0 \approx 10^{-18}$ cm^2, $\hbar\omega$ is photon energy, ε_0 is CTE energy, $A \approx 10^{-2}$ eV is Stokes shift and $\Delta \approx 10^{-2}$ eV is bandwidth. We consider a linear polarized wave and use the well-known formula for absorption band of an impurity center at strong electron–phonon coupling. A second exciton is generated in the electric field of the first exciton, therefore its energy ε_i, and hence generation rate W_i, depends on its relative position with respect to the first CTE (i is the number of the cell where a new exciton is generated). In general, case energy of the generated exciton depends on its position and the dependence is determined by the positions of the excitons available:

$$\varepsilon_i = \varepsilon_0 + \sum_j V_{ij},$$

where $\sum_j$ is taken over by existing excitons and contributes to the exciton energy due to interaction with other excitons

$$V_{ij} = \frac{d^2(1 - 3\cos^2\theta_{ij})}{|\mathbf{R}_i - \mathbf{R}_j|^3},$$

where $\mathbf{R}_i$ and $\mathbf{R}_j$ are the exciton positions, θ_{ij} is the angle between the exciton dipole moment $\mathbf{d}$ and radius-vector between the interacting particles $\mathbf{R}_i - \mathbf{R}_j$ (all excitons have the same dipole moment $\mathbf{d}$). So, the energy of the exciton and therefore the probability of its generation

$$W_i = I\sigma_0 \exp\left[-(\hbar\omega - \varepsilon_i - A)^2/\Delta^2\right]$$

depends on the positions of already existing excitons and this is the reason for the ordering. Indeed, if photons are resonant to the first exciton

$$\hbar\omega - \varepsilon_0 - A = 0$$

and CTE is generated in the cell j there is some part of this cell where resonance conditions are broken by interactions $\sum_j V_{ij}$, so that CTE energy

$$\varepsilon_i = \varepsilon_0 + \sum_j V_{ij}$$

is out of resonance and excitons are not generated. This correlation between generation rate at some point and the distribution of already existing particles is the mechanism of the self-organization. Absorbed photons generate the electron excitation and a phonon and phonon's break phase relations in the exciton wave function, therefore nondiagonal elements of the density matrix become negligible. The simplest rate equations for probability of the exciton population of different cells ρ_i are valid in this case

$$\frac{\mathrm{d}\rho_i}{\mathrm{d}t} = I\sigma_0 \exp\left[-(\hbar\omega - \varepsilon_i - A)^2/\Delta^2\right] - \gamma\rho_i,$$

where t is time, $\gamma \approx 10^8\ \mathrm{s}^{-1}$ is decay constant and $\rho_i \ll 1$. Dipole–dipole interaction is too complicated: it depends on spatial angles and is long range in a three-dimensional system. We will take these peculiarities into account a little bit later. As a first step in our study, let's consider static solutions of the above rate equations for close-neighbor interaction $V_{ij} = V$. We can find a static solution for the equation

$$\rho_i = \mu \exp\left[-\left(\xi - \alpha \sum_j \rho_j\right)^2\right]$$

graphically. Here cells i, j are neighbors,

$$\mu = I\sigma_0/\gamma, \qquad \xi = (\hbar\omega - \varepsilon_0 - A)/\Delta, \qquad \alpha = V/\Delta.$$

There is solution $\rho_i = \text{const}$ at any pumping. At $\mu > 1$ (photon flux is $I > 10^{26}\ \mathrm{s}^{-1}\,\mathrm{cm}^{-2}$, which corresponds to light power $>10^7\ \mathrm{W\ cm}^{-2}$) exciton density forms a superlattice with period $2a$ in the case considered, where a is a period of the crystal. Any cell with the probability of exciton population ρ_1 is surrounded by the cells with another population ρ_2 and vice versa, therefore

$$\rho_1 = \mu \exp\left[-(\xi - 2p\alpha\rho_2)^2\right],$$
$$\rho_2 = \mu \exp\left[-(\xi - 2p\alpha\rho_1)^2\right],$$

where p is the dimensionality of the system. Homogeneous ($\rho_1 = \rho_2$) and inhomogeneous ($\rho_1 \neq \rho_2$) solutions of the system of the above transcendent equations are presented in Fig. 2.1.

Inhomogeneous solutions appear at high pumping, $\mu > 1$, and present spatial ordering of the excitons: they form a double-component superlattice where two values of population probability alternate in space like charges in NaCl-crystal. Our study of stability shows that these states are stable at high pumping while the homogeneous states $\rho_1 = \rho_2$ become unstable [12].

New solutions at the pumping I_2 (Fig. 2.1) arise when one curve touches the other; this is similar to the new phase formation in a second-order phase transition. The new phase is absent above temperature T_c and it emerges at temperature $T < T_\mathrm{c}$. Analogous to this behavior, the light-induced ordering takes place when the light's power exceeds some threshold: $\mu > \mu_0$.

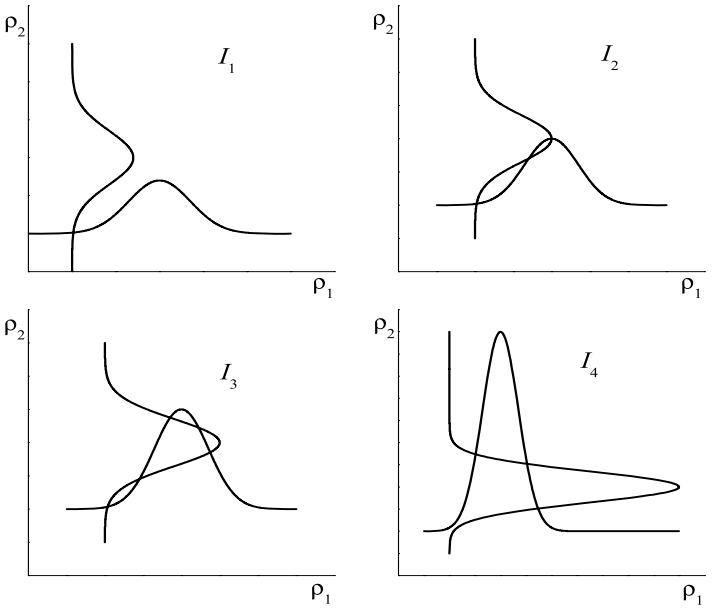

Fig. 2.1. Possible homogeneous ($\rho_1 = \rho_2$) and inhomogeneous ($\rho_1 \neq \rho_2$) states for different pumping $I_1 < I_2 < I_3 < I_4$

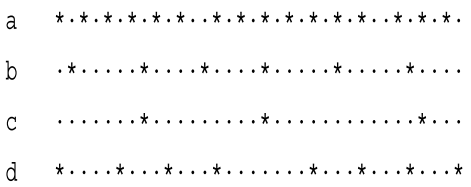

Fig. 2.2. Distribution of excitons (∗) about the sites in the case of dipole–dipole interaction at the following parameter values: **a** $\xi = 1$, $\alpha = 10$, $\mu = 500$; **b** $\xi = 0$, $\alpha = 100$, $\mu = 500$; **c** $\xi = 0$, $\alpha = 10^3$, $\mu = 10^2$; **d** $\xi = 3$, $\alpha = 100$, $\mu = 100$

It is interesting to observe the superlattice formation via a computer experiment. This method can give only stable states because digital noise serves as perturbation, which breaks the unstable state so that only stable ones survive. Each cell can be in a ground or excited state ($n_i = 0$ or $n_i = 1$, respectively). If at moment of time t a series of sites are excited during the next time interval $\mathrm{d}t$, each excitation can randomly annihilate with the probability $\gamma\,\mathrm{d}t \ll 1$ and a cell in ground state—also randomly with the probability $W_i\,\mathrm{d}t \ll 1$—can transit into an excited state. The excitation rate W_i was calculated with regard to distribution of excitons at the moment t. It is interesting to observe the intermediate information on display. At small pumping $\mu \ll 1$, as was expected, the exciton distribution over the sites is chaotic. At $\mu \to 1$, clusters of ordered states appear as shown in Fig. 2.2.

Excitons are packed into a superlattice, and a new period appears in the system. Its origin can be understood from the following. If cell j is excited, then each new exciton in cell i has addition to the energy

$$V_{ij} = \frac{d^2}{|\mathbf{R}_i - \mathbf{R}_j|^3}$$

(the system is one-dimensional and the dipole moments are perpendicular to the chain). For long distances $|\mathbf{R}_i - \mathbf{R}_j|$ the interaction is negligible. It becomes important when the addition equals the CTE absorption bandwidth Δ. This condition

$$\frac{d^2}{|\mathbf{R}_i - \mathbf{R}_j|^3} = \Delta$$

gives an estimation for the superlattice period

$$R = \left(d^2/\Delta\right)^{1/3},$$

or

$$R = a\left(d^2/a^3\Delta\right)^{1/3} \approx 10a,$$

where a is a lattice constant of the molecular crystal. Note the key role played by the absorption bandwidth Δ, which you never see in thermodynamically built crystal. The correlation function

$$K_{ij} = \langle n_i n_j \rangle \equiv \frac{1}{T}\int_0^T \mathrm{d}t n_i(t) n_j(t) - \langle n \rangle^2$$

demonstrates the spatial ordering of the excitons at high pumping (Fig. 2.3). Here $\langle n_i n_j \rangle$ is the time average of the population numbers $n_i n_j$ product in the stationary state,

$$\langle n \rangle \equiv \langle n_i \rangle = \frac{1}{T}\int_0^T \mathrm{d}t n_i(t) \equiv \rho,$$

where ρ is the exciton concentration.

The storage time $T = 100$ was not long enough, therefore long-lived defects with life spans at about the same value spoiled the right-hand part of the correlation function. At $T \to \infty$ the calculation should give, of course, a symmetric function K_{ij}. It can be found analytically for one-dimensional lattice and nearest neighbor interaction at high power limit $\mu \gg 1$ when superlattice is close to ideal. Note that

$$K_{ij} = \langle n_i n_j \rangle = K_{ij}^{(0)}(1 - \rho_\mathrm{d})^{|i-j|},$$

where $K_{ij}^{(0)}$ is a correlation function for ideal crystal (it oscillates without decay),

$$\rho_\mathrm{d} = n_\mathrm{d}/N \ll 1$$

is the concentration of defects, n_d is the number of defects and N is the number of cells. Factor

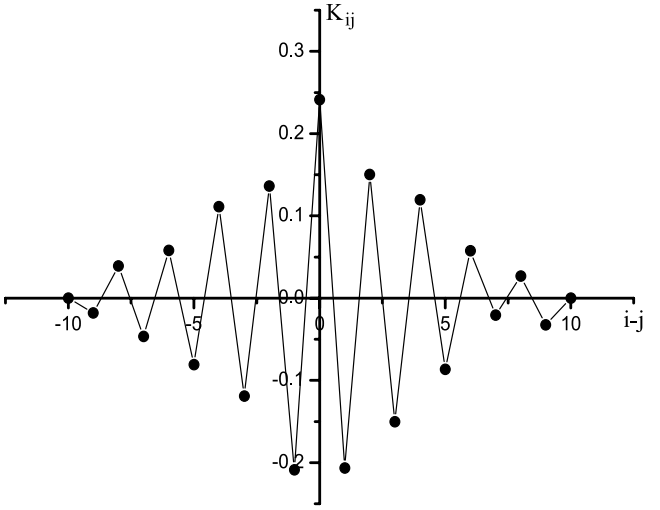

Fig. 2.3. The correlation function $K_{ij} = 1/T \int n_i(\tau) n_j(\tau)\,\mathrm{d}\tau - \rho^2$ at $\xi = 1$, $\alpha = 10$, $\mu = 100$ (interactions of closest neighbors, the integral is taken from 100 to $100 + T$, $T = 100$)

$$(1 - \rho_\mathrm{d})^{|i-j|}$$

means that there are no defects between sites i and j. As far as

$$(1 - \rho)^{1/\rho} \to \mathrm{e}$$

is concerned, at $\rho \to 0$ the correlation function becomes

$$K_{ij} = K_{ij}^{(0)} \exp(-\rho_\mathrm{d}|i - j|).$$

Defects are generated in ideal superlattice 10101010 by two CTE decays and one CTE generation in the wrong position

$$10101010 \to 10001010 \to 10000010 \to 10010010.$$

After that, two ideal pieces are separated by two neighboring domain walls. A single wall separates two pieces shifted in space to lattice constant 010101001010 10. The probability W_d of this defect generation during time T is calculated directly. The probability of CTE generation consists of following factors: the probability that CTE did not decay up to time t' (equal to $\exp(-\gamma t')$) and CTE decay during the next time interval $\mathrm{d}t'$ (equal to $\gamma\,\mathrm{d}t'$) and the analogous factors corresponding to decay of the next CTE at time interval $\mathrm{d}t''$ and generation of CTE in the wrong position at time interval $\mathrm{d}t'''$:

$$W_\mathrm{d} = 2 \int \gamma \mathrm{d}t' \exp(-\gamma t') \int \gamma \mathrm{d}t'' \exp\bigl[-(\gamma + W)(t'' - t')\bigr]$$
$$\times \int W \mathrm{d}t''' \exp\bigl[-3W(t''' - t'')\bigr] = \frac{2\gamma^2 T}{3W}$$

at $W \gg \gamma$.

Here W is the CTE generation rate. The three above integrals are taken in time intervals $(0, T)$, (t', T) and (t'', T), respectively, and are the sum over all above-stated events. A single domain wall in bulk can move only, but cannot annihilate. This may happen when a domain wall meets another wall, therefore the rate of defect decay consists of two factors: $(n_\mathrm{d}/N)\gamma$ = (probability to find neighboring defect) (CTE decay rate).

Equilibrium condition in generation and annihilation of the defects

$$N\frac{2\gamma^2}{3W} = n_\mathrm{d}\frac{n_\mathrm{d}}{N}\gamma$$

gives the estimation for the defect concentration

$$\rho_\mathrm{d} \equiv \frac{n_\mathrm{d}}{N} \approx \left(\frac{\gamma}{W}\right)^{1/2} = \left(\frac{\gamma}{I\sigma_0}\right)^{1/2}$$

at resonance condition $\xi = 0$, and $\alpha \gg 1$, $\mu \gg 1$. We have finally for the correlation function

$$K_{ij} = K_{ij}^{(0)} \exp\left[-\left(\frac{\gamma}{I\sigma_0}\right)^{1/2} |i - j|\right],$$

which is in agreement with the above computer simulation. The system tends to reach an ideal superlattice at $\gamma/I\sigma_0 \to 0$. We observed this behavior for two dimensions in computer experiments. The ideal superlattice looks like a chess board in this case. There are two ideal states: one of them is shifted to lattice constant with respect to another (white and black sites are changed). At the first stage of our computer simulation, a lot of these pieces are generated, divided by domain walls. Domain walls are now closed curves inside the sample or they go from boundary to boundary. These walls move, changing the size of the domain. Small pieces decrease and disappear, but big pieces increase and spread over all the sample, as shown in Fig. 2.4. Excited cells are white (occupation numbers are $n = 1$); unexcited cells are black. One can see in Fig. 2.4 a nice tendency of the self-organized system to approach an ideal state.

2.1.2 Orientational Ordering

If electron transfer from donor to acceptor is possible in both directions, then each cell can be in *three* states: one ground state ($n_i = 0$) and two excited states with different orientation of CTE dipole moment ($n_i = \pm 1$). Both the energy of the generated exciton and the probability of generation depend on its position and dipole moment orientation. So, the probability of CTE generation in some cell with some dipole moment orientation depends on positions and dipole moment orientation of the excitons available. This correlation results in spatial as well as orientational ordering.

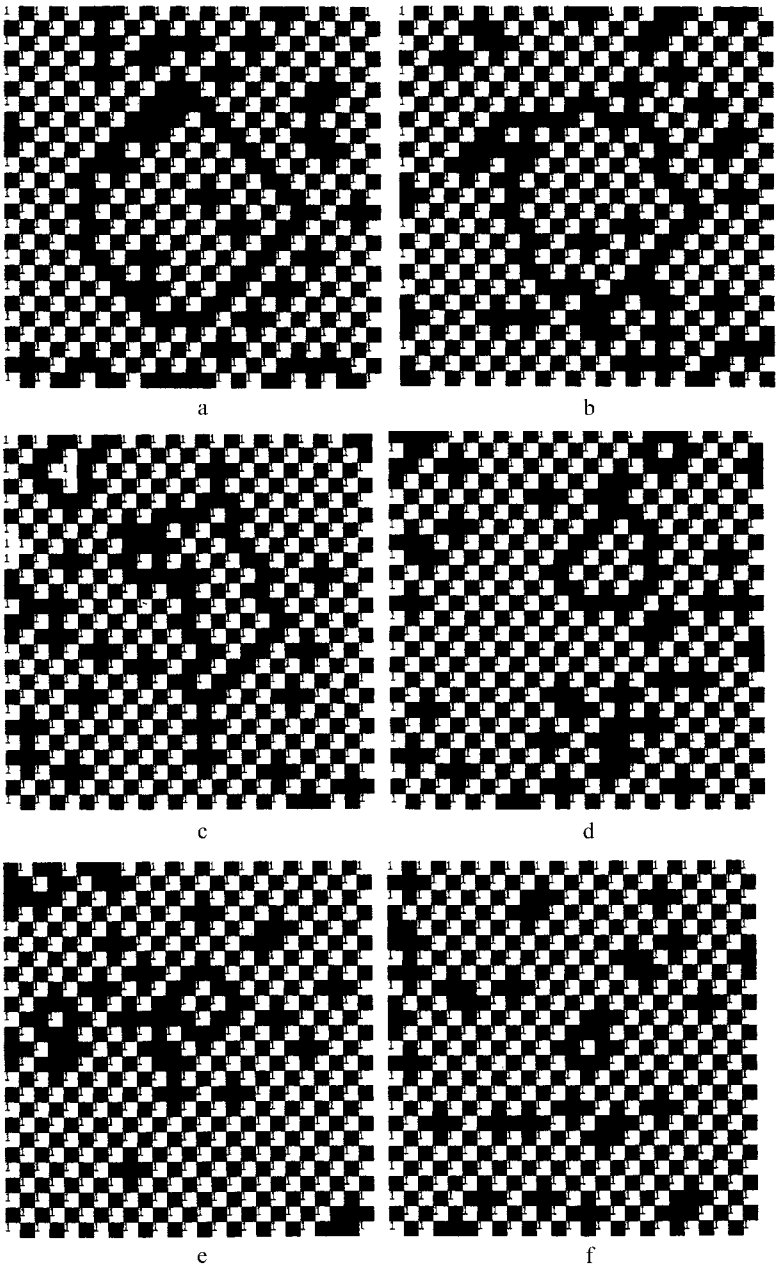

Fig. 2.4. Ostracism of the defect: decrease and disappearance of the small domain and increase of big domain. Snaps at $\tau = 0.5$ (**a**), $\tau = 8$ (**b**), $\tau = 25.5$ (**c**), $\tau = 41.5$ (**d**), $\tau = 47$ (**e**), $\tau = 52$ (**f**) ($\xi = 0$, $V/\Delta = 5$, $\mu = 10$, two-dimensional lattice)

The exciton energy is now

$$\varepsilon_i = \varepsilon_0 + \sum_j V_{ij} n_i n_j,$$

where V_{ij} is again

$$V_{ij} = \frac{d^2(1 - 3\cos^2\theta_{ij})}{|\mathbf{R}_i - \mathbf{R}_j|^3}.$$

The generation rate now depends on the generated exciton position i and its dipole moment orientation n:

$$W_{ni} = I\sigma_0 \exp\left[-\left(\hbar\omega - \left(\varepsilon_0 + n_i \sum_j V_{ij} n_j\right) - A\right)^2 \Big/ \Delta^2\right];$$
$$n = n_i = \pm 1.$$

Let ρ_{ni} be the probability of state ni occupation; then in self-consistent approximation the rate equation is

$$\frac{\mathrm{d}\rho_{ni}}{\mathrm{d}t} = I\sigma_0 \exp\left[-\left(\hbar\omega - \varepsilon_0 - n \sum_{n'j} V_{ij} n' \rho_{n'j} - A\right)^2 \Big/ \Delta^2\right] - \gamma\rho_{ni}.$$

The sum

$$\sum_{n'} n' \rho_{n'j} \equiv d_j$$

is the average dipole moment of the site j measured in d units. For the variables d_j the equation may be rewritten as

$$\frac{\mathrm{d}d_i}{\mathrm{d}\tau} = \mu \exp\left[-\left(\xi - \sum_j \alpha_{ij} d_j\right)^2\right] - \mu \exp\left[-\left(\xi + \sum_j \alpha_{ij} d_j\right)^2\right] - d_j,$$

where

$$\alpha_{ij} = V_{ij}/\Delta,$$

and temporal derivative $\frac{\mathrm{d}}{\mathrm{d}\tau}$ is taken over dimensionless time

$$\tau = \gamma t.$$

The dipole moments now reveal spatial self-organization together with orientational ordering. In the competition between different possible states we can find static solutions of the rate equation for nearest neighbor interaction $\alpha_{ij} \equiv \alpha$. There is the state where each dipole moment d_1 is surrounded by dipole moments d_2 and vice versa, then for the values d_1 and d_2 we have equations

$$d_1 = \mu \exp\left[-(\xi - 2p\alpha d_2)^2\right] - \mu \exp\left[-(\xi + 2p\alpha d_2)^2\right],$$
$$d_2 = \mu \exp\left[-(\xi - 2p\alpha d_1)^2\right] - \mu \exp\left[-(\xi + 2p\alpha d_1)^2\right],$$

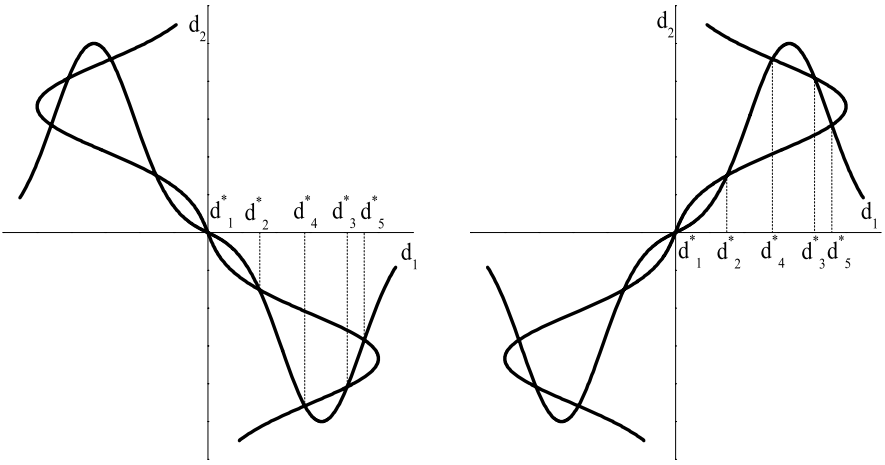

Fig. 2.5. Possible states: $\xi/\alpha < 0$, antiferroelectric-type ordering (first graph); $\xi/\alpha > 0$, ferroelectric-type ordering (second graph)

where p is dimensionality of the system. Graphical solutions of the system are shown in Fig. 2.5.

Figure 2.5 presents ferroelectric and antiferroelectric ordering of the system. Ferroelectric-type ordering corresponds to the state with the same orientation of dipole moments in all unit cells. In the antiferroelectric state, the directions of dipole moments in neighboring cells are opposite. The values of dipole moments in different cells may be the same (solutions d_1^*, d_2^*, d_3^*) or different (solutions d_4^*, d_5^*). Figure 2.5 exhibits both spatial (crystal like) and orientational ordering of CTE dipole moments. Note that we investigated action of a linear polarized light wave; therefore, initial molecular crystal and light waves have the inversion symmetry which is lost spontaneously in the ordering process. This is analogous to ferroelectric or magnetic phase transition. Light intensity is a governed parameter in self-organization, similar to temperature in the phase transition. Our consideration is insensitive to the form of the absorption band and to the type of the interaction. We shall see, in all cases, the universality of the self-organization and its independence of the details. This is quite analogous to the universality of the second-order phase transition. Calculation of the response to static electric field, presented later, shows negative susceptibility to disordered state or positive feedback in the response. The initial field is amplified by ordered dipole moments and the disordered state transits to the ordered state. Ferroelectric ordering results in macroscopic polarization, which changes the optical properties of a material. These peculiarities will be considered in detail later.

2.2 Ordering in Random Impurity System

The internal life of the self-organized system may be observed in optical experiments. As we have seen, the excitation of some cells changes cross-section of the

light absorption of the other cells. This means that direct measurement of the temporal variation of the light transmitted through a sample manifests time dependence of the site populations. We shall see by direct observation breather of a matter. Polarization of a sample also strongly fluctuates. It is observed in measuring the rise of the second harmonic signal. Polarization and the signal reveal universal $1/\omega$ spectrum. We shall see this characteristic spectrum in numerous measurements and in the corresponding calculations. In any case it means that the studied process belongs to the class of the self-organized phenomena.

We examine here time evolution of N active centers randomly distributed in three-dimensional space. Let each center i be in ground state ($n_i = 0$) and 10 excited states with dipole moments $d_i = n_i d$, $-5 \le n_i \le 5$, corresponding to different charge transfer distance $R_i = n_i a$. The excitation rate decreases with transfer range R exponentially $\propto \exp(-\kappa R)$, but this does not mean that long-range excitons play minor roles. Their decay rate is decreased to the same factor and the stationary population does not depend on this sharp factor at all. It influences kinetics only: long-range excitons are created slowly and are long-lived. If the light pumping is switched off, the short-distance CTEs decay but long-distance excitons survive. In addition, they have a large dipole moment and therefore dominate in macroscopic polarization. I shall consider

$$\kappa = 1/a,$$
$$\exp(-\kappa R) = \exp(-|n_i|)$$

and rewrite the probability of CTE generation in the form

$$W_{ni} = I\sigma_0 \exp\left[-|n| - \left(\hbar\omega - \varepsilon_0 - n\sum_j V_{ij} n_j - A\right)^2 \Big/ \Delta^2\right].$$

This formula gives the CTE generation rate of the state $n = n_i$ at site i dependent on spatial distribution and states of others excitons. The corresponding decay rate is

$$\gamma_0 \exp(-|n_i|).$$

We performed computer simulation of CTE generation and annihilation for 800 impurities randomly introduced into a three-dimensional lattice $200 \times 200 \times 200$ in size (in lattice constant units $a = 5 \times 10^{-8}$ cm). It was found that at weak light pumping, $\mu \ll 1$, the behavior of the system is linear. Total light absorption shows photobleaching and is constant in time with normal relative fluctuation $N_e^{-1/2}$, where N_e is number of excitons. At high light pumping, $\mu \ge 1$, the system becomes strongly nonlinear. At constant pumping the system never attains stationary state; it is constantly in motion. As a result, light absorption and macroscopic polarization become time dependent. The total cross-section σ_t of resonance photons

$$\hbar\omega - \varepsilon_0 - A = 0$$

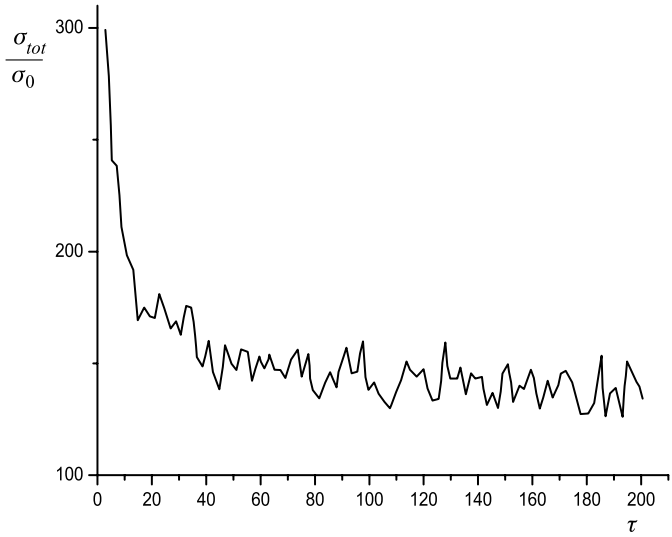

Fig. 2.6. Time dependence of the cross-section of photon absorption for resonant light $\hbar\omega - \varepsilon_0 - A = 0$, $\mu = 2$, $d_0^2/\Delta a^3 = 100$, $N = 800$

was calculated as a sum over all nonexcited states at each time moment

$$\sigma_t = \sum_{ni} \sigma_0 \exp\left[-|n| - \left(n \sum_j V_{ij} n_j\right)^2 \Big/ \Delta^2\right]$$

and is shown in Fig. 2.6.

It takes into account all possible absorption processes forming the CTE absorption band; in other words the total cross-section. The observed fluctuation exceeds considerably the normal level $N_e^{-1/2}$. Transmitted light should fluctuate in the same manner. Time dependence of total dipole moment (macroscopic polarization) is shown in Fig. 2.7.

It strongly fluctuates with the $1/\omega$ spectrum as $\omega \to 0$, shown in Fig. 2.8. Macroscopic polarization P induces second-order nonlinear susceptibility $\chi^{(2)} \propto P$; therefore, the efficiency of the frequency doubling would fluctuate with the same spectrum.

It is interesting that the induced polarization fluctuating around zero level for our small system (Fig. 2.7) can be oriented by external electric field and proper choice of the light frequency. If the photon energy exceeds the maximum of the linear absorption band (the band at the absence of other excitons)

$$\hbar\omega > \varepsilon_0 + A,$$

then generating the exciton with dipole moment in opposition to the local electric field is preferable to generating the exciton with dipole moment aligned with the field. This is because the field contribution to the energy is positive and it shifts

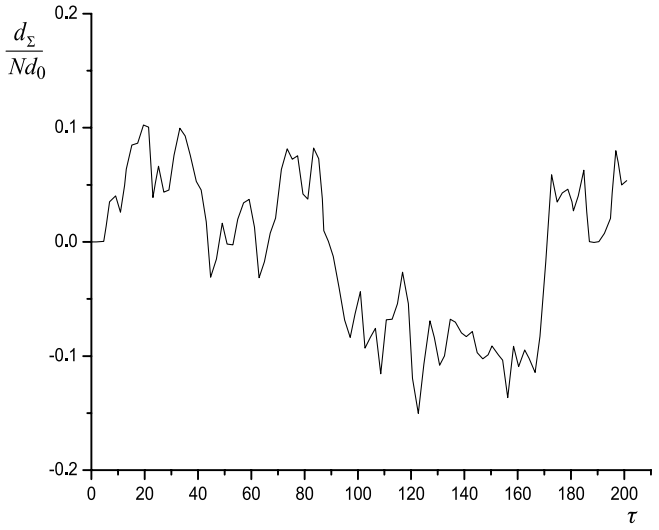

Fig. 2.7. Time dependence of total dipole moment d_Σ ($\hbar\omega - \varepsilon_0 - A = 0$, $\mu = 2$, $d_0^2/\Delta a^3 = 100$, $N = 800$)

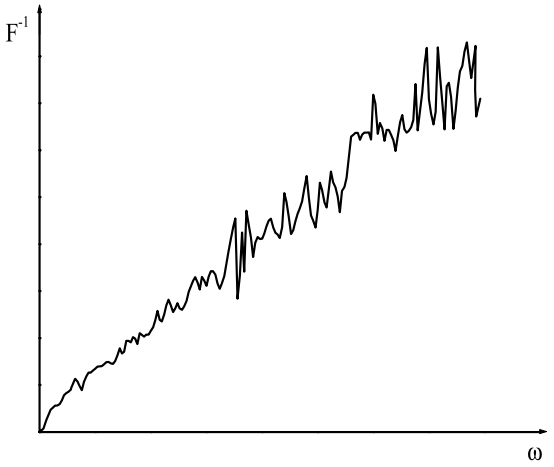

Fig. 2.8. The Fourier transform of $d_\Sigma(\tau)$ dependence: $1/\omega$ noise

the level to resonance. In contrast, the dipole moment in the direction of the local electric field decreases the exciton energy and shifts it away from resonance. As a result, total sample polarization is oriented opposite to the external electric field which corresponds to the positive feedback or negative susceptibility, as already discussed. We see again that light works like an optical motor: it prepares the high-energy state, intensively building the ordered structure. In a closed thermodynamic

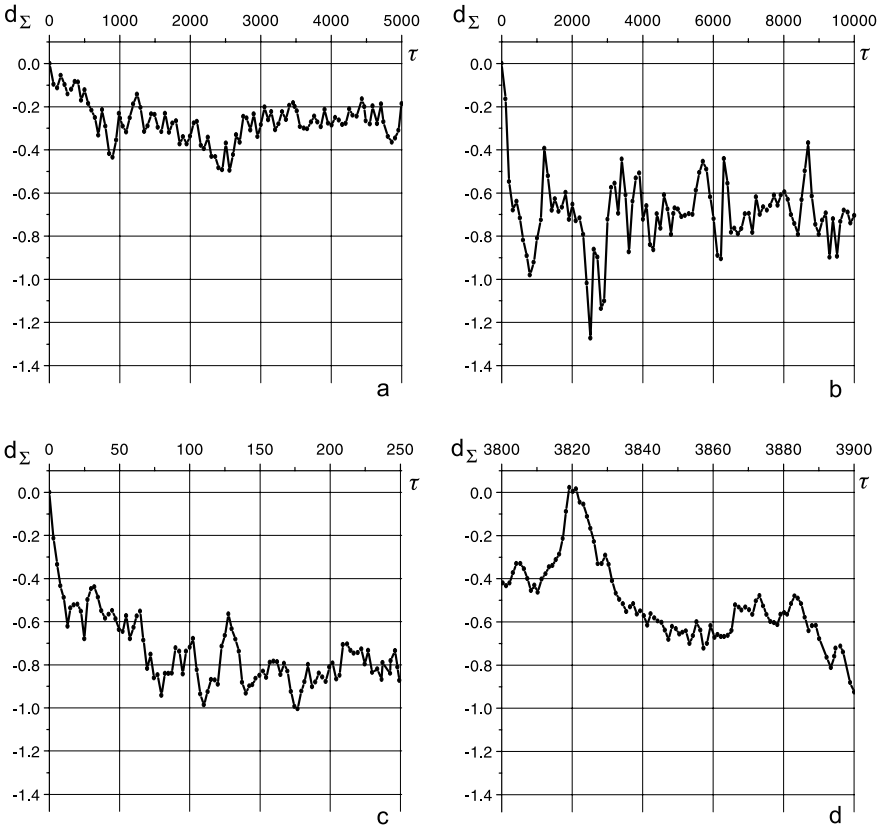

Fig. 2.9. Time evolution of normalized dipole moment $d_\Sigma(\tau)$ for $\xi = 1$, $d_0^2/\Delta a^3 = 100$, $\widetilde{E}_0 = 0.1$, $N = 100$, sample size is $100 \times 100 \times 100$. **a** $\mu = 0.05$, averaging over time interval $\delta\tau = 50$; **b** $\mu = 1$, $\delta\tau = 100$; **c** $\mu = 20$, $\delta\tau = 2.5$; and **d** $\mu = 1$ (in detail, $\delta\tau = 1$)

system, on the other hand, low-energy states are predominate and this corresponds to the normal negative feedback or positive susceptibility.

The results of our computation are shown in Figs. 2.9 and 2.10. Noise is presented in all spectral ranges (Fig. 2.9). Light-driven kinetics in the external field exhibit preparation of the polarized state: symmetric exciton states d_n and d_{-n} are populated differently. States d_{-1}, d_{-2}, d_{-3}, d_{-4}, d_{-5} (with dipole moments oriented opposite to the external field $\widetilde{E}_0 > 0$ direction and positive field contribution to the excitation energy $-\mathbf{d}_{-n}\mathbf{E} > 0$) are populated predominantly in comparison with the corresponding states d_1, d_2, d_3, d_4, d_5 ($-\mathbf{d}_{-n}\mathbf{E} < 0$).

Our system is strongly nonlinear and nonlinear effects are responsible for the behavior of the system. They cannot be considered by perturbation theory of any kind, therefore analytic study of the system is extremely difficult. We can propose a "theorem": there is no self-organization in the system that allows rigorous analytic study. This is the reason a lot of computer simulations and figures obtained by

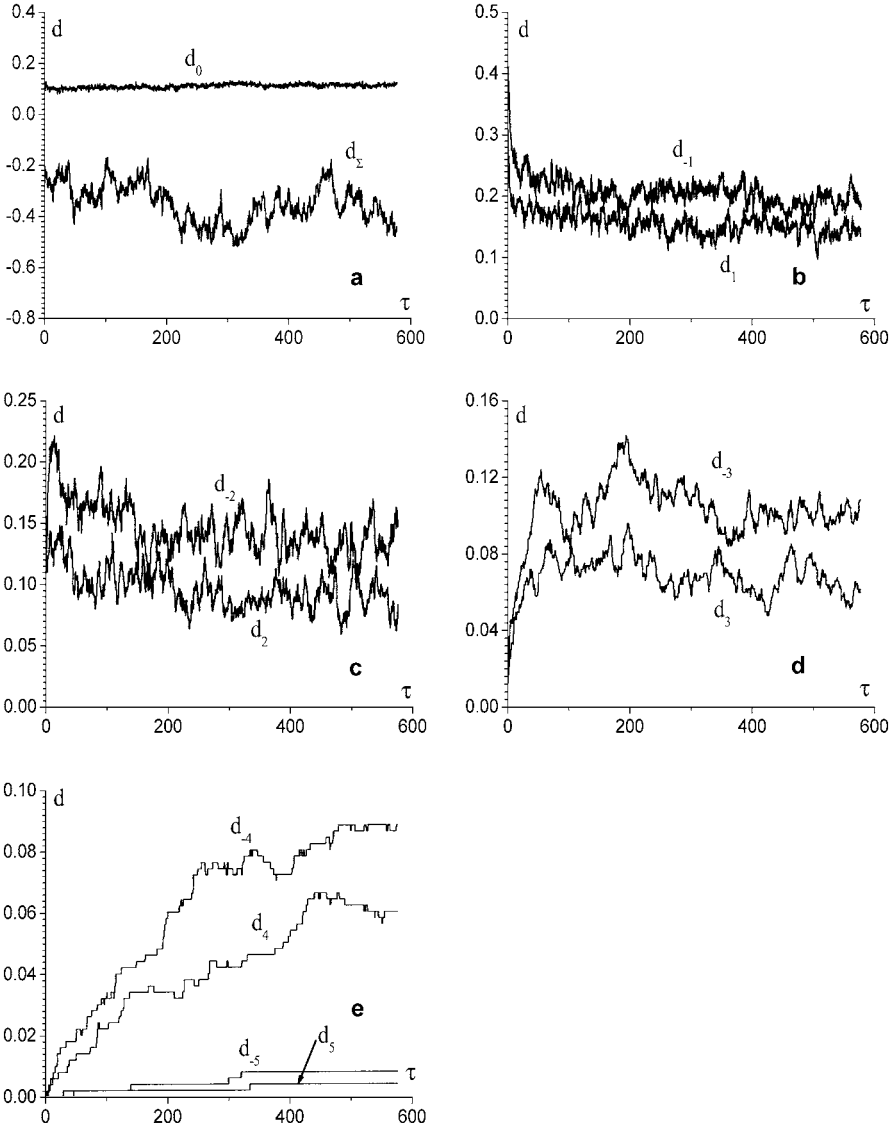

Fig. 2.10. Time dependence of dipole moment $d_\Sigma(\tau)$ and fractions of centers $d_m(\tau)$ in state m ($\sum d_m(\tau) = 1$) for $\mu = 10$, $\xi = 1$, $d_0^2/\Delta a^3 = 100$, $\widetilde{E}_0 = 0.1$, $N = 500$, sample size is $400 \times 50 \times 50$, $\delta\tau = 0.4$. **a** d_0, d_Σ; **b** d_1, d_{-1}; **c** d_2, d_{-2}; **d** d_3, d_{-3}; **e** d_4, d_{-4}, d_5, d_{-5}

computer experiment are presented here. Fortunately, it is easy to find results using a self-consistent approach. The more difficult problem is to explain why it works. We compared results of self-consistent study and computer simulations and found them to be in good agreement. This is analogous to the well-known fact that Landau mean field theory of phase transitions is even better than it should be: it can be used, for example, to describe the displacement-type structure phase transitions where, rigorously speaking, it should not work.

The average dipole moment of the active center in the homogeneous ferroelectric state may be written in the following way

$$\langle d_i \rangle = \langle n_i \rangle d \equiv \langle n \rangle d,$$

where

$$\langle n \rangle = \sum_n \rho_{ni}.$$

Macroscopic polarization (total dipole moment of 1 cm^3) is proportional to this variable

$$P = c' \langle n \rangle d,$$

where c' is concentration of active centers (cm^{-3}). This polarization results in the corresponding static electric field

$$E = -4\pi P \equiv -4\pi c' \langle n \rangle d$$

for plain geometry. Energy of CTE in state n (dipole moment $n_i d$) in this field is

$$\varepsilon_i = \varepsilon_0 - n_i d(E + E_0) = \varepsilon_0 - n_i d(-4\pi c' \langle n \rangle d + E_0)$$

(E_0 is external electric field). The rate equations become

$$\frac{\mathrm{d}\rho_{ni}}{\mathrm{d}t} = I\sigma_0 \exp\left[-|n_i| - \left(\hbar\omega - \varepsilon_0 - A + n_i d(-4\pi c' \langle n \rangle d + E_0)\right)^2 / \Delta^2\right] - \gamma_0 \exp(-|n_i|)\rho_{ni},$$

or for the static case

$$\rho_{ni} = \mu \exp\left[-\left(\xi - 4\pi c' n_i \langle n \rangle d^2/\Delta + n_i d E_0/\Delta\right)^2\right].$$

Taking into account the definition for $\langle n \rangle$, we have the self-consistent equation for the variable $\langle n \rangle$

$$\langle n \rangle = \sum_{n>0} n\mu \left[\exp\left[-\left(\xi - 4\pi c' n \langle n \rangle d^2/\Delta + n d E_0/\Delta\right)^2\right] - \exp\left[-\left(\xi + 4\pi c' n \langle n \rangle d^2/\Delta - n d E_0/\Delta\right)^2\right]\right].$$

A small deviation from the state $\langle n\rangle = 0$ at $E_0 \to 0$ is found by expanding the exponents

$$\langle n\rangle = \mu \mathrm{e}^{-\xi^2}\left[\sum_n n^2\right]\left[16\pi\xi\langle n\rangle c' d^2/\Delta - 4\xi d E_0/\Delta\right],$$

and we find finally the self-consistent solution

$$\langle n\rangle = \mu \mathrm{e}^{-\xi^2}\left[\sum_n n^2\right][-4\xi d E_0/\Delta]\left[1 - \mu \mathrm{e}^{-\xi^2}\left[\sum_n n^2\right]16\pi\xi c' d^2/\Delta\right]^{-1}.$$

Sum $\sum_n n^2$ is taken over all states' attained stationary conditions

$$t I \sigma_0 \mathrm{e}^{-|n_i|} \gg 1,$$
$$t\gamma \mathrm{e}^{-|n_i|} \gg 1.$$

Another restriction rises from violation of the dipole–dipole interaction at large $|n_i|$. The dominant role of the long-range states is seen from the earlier considerations. Insofar as $\langle n\rangle$ is the average dipole moment of the site in d units, the last formula gives the susceptibility of the system under light pumping. It is negative at $\xi > 0$ (positive feedback) and diverges with increased pumping, which manifests instability of the state $\langle n\rangle = 0$ and further transition to polarized state. The reader is referred to [13] for all details and corresponding references to the problem.

It is interesting that, due to the nonlinear behavior of our system, it may emit photons with higher energy than the absorbed photons. For example, let the first photon be resonant to an electron transition

$$\hbar\omega_1 = \varepsilon_0 + A,$$

and generate the first charge transfer exciton (CTE) with dipole moment **d**. Assume that the second photon generates the second CTE with dipole moment $-\mathbf{d}$ at the distance $2a$ from the first exciton in perpendicular to **d** direction. This excitation needs energy

$$\hbar\omega_2 = \varepsilon_0 + A - \frac{d^2}{(2a)^3}.$$

Let the third CTE with dipole moment **d** be generated between the first and the second CTE. The resonance photon energy is

$$\hbar\omega_3 = \varepsilon_0 + A.$$

If the second exciton decays, then the emitted photon energy is

$$\hbar\widetilde{\omega}_1 = \varepsilon_0 - A - \frac{d^2}{a^3} - \frac{d^2}{(2a)^3}.$$

The next decay generates photon

$$\hbar\widetilde{\omega}_2 = \varepsilon_0 - A + \frac{d^2}{a^3},$$

and photon

$$\hbar\widetilde{\omega}_3 = \varepsilon_0 - A$$

is emitted during the last decay.

The energy of the second photon $\hbar\widetilde{\omega}_2$ exceeds considerably the absorbed photon energies $\hbar\omega_1$, $\hbar\omega_2$ and $\hbar\omega_3$.

Here

$$A \approx 0.01 \text{ eV},$$
$$\frac{d^2}{a^3} \approx 1 \text{ eV}.$$

Total absorbed energy is

$$\hbar\omega_1 + \hbar\omega_2 + \hbar\omega_3 = 3\varepsilon_0 + 3A - \frac{d^2}{8a^3},$$

while total emitted energy is

$$\hbar\widetilde{\omega}_1 + \hbar\widetilde{\omega}_2 + \hbar\widetilde{\omega}_3 = 3\varepsilon_0 - 3A - \frac{d^2}{8a^3}.$$

Energy is conserved with the accuracy

$$A \ll \varepsilon_0,$$
$$A \ll \frac{d^2}{a^3},$$

but the redistribution of the energy between photons happens: the first photon received minimum energy $\hbar\widetilde{\omega}_1$, but the second one gained maximum energy $\hbar\widetilde{\omega}_2$. Direct calculation of the emission spectrum shows that indeed high-energy bands do exist and their energies exceed the absorbed photon energies. More exact calculation of the discussed three-photon energy reveals energy lost $6A$. It is supplied to the atom vibrations and the loss is A at each photon absorption or emission.